Enhancing the localization of uterine leiomyomas through cutaneous softness rendering for robot-assisted surgical palpation applications

Davide Doria[†] Simone Fani[†] Andrea Giannini[††] Tommaso Simoncini[††] Matteo Bianchi[†,‡‡]

***Abstract*—Integrating tactile feedback for lump localization in Robot-assisted Minimally Invasive Surgery (RMIS) represents an open research issue, which is still far to be solved. Main reasons for this are related e.g. to the need for a transparent connection with the teleoperating console, and an intuitive decoding of the delivered information. In this work, we focus on the specific case of RMIS treatment of uterine leiomyomas or fibroids, where little has been done in haptics to improve the outcomes of robotics-enabled palpation tasks. In this paper, we propose the usage of a wearable haptic interface for softness rendering as a lump display. The device was integrated in a teleoperation architecture that simulates a robot-assisted surgical palpation task of leiomyomas. Our work moved from an *ex-vivo* sample characterization of uterine tissues to show the effectiveness of our interface in conveying meaningful softness information. We extensively tested our system with gynecologic surgeons in palpation tasks with silicone specimens, which replicated the characteristics of uterine tissues with embedded leyomiomas. Results show that our system enables a softness-based discrimination of the embedded fibroids comparable to the one that physicians would achieve using directly their fingers in palpation tasks. Furthermore, the feedback provided by the haptic interface was perceived as comfortable, intuitive, and highly useful for fibroid localization.**

I. Introduction

Uterine leiomyomas, also known as uterine fibroids or myomas, are benign tumors that can be located on the surface of the uterus (subserous fibroids) or within the muscle tissue of the uterus (intramural fibroids). Under a physical and mechanical point of view, myomas usually appear as hard lumps in the uterine tissues, whose stiffness is typically higher with respect to the one of the surrounding tissues [1], [2]. The estimated prevalence is of up to 15-50% in women older than 53 years. About 80% of women affected by fibromatosis have symptoms (which include bleeding, menstrual and pelvic pain and infertility) and require treatment, which usually consists of surgical ablation, such as hysterectomy [3] or myomectomy [4].

State of the art surgical therapy for myoma treatment strongly relies on the usage of commercial robotic platforms for Robot-assisted Minimally Invasive Surgery (RMIS), such as the da Vinci Xi surgical system (Intuitive Surgical, CA, USA)[1] [5], which target the removal of the uterine fibroid or, in a precautionary manner, of the whole uterus [6].

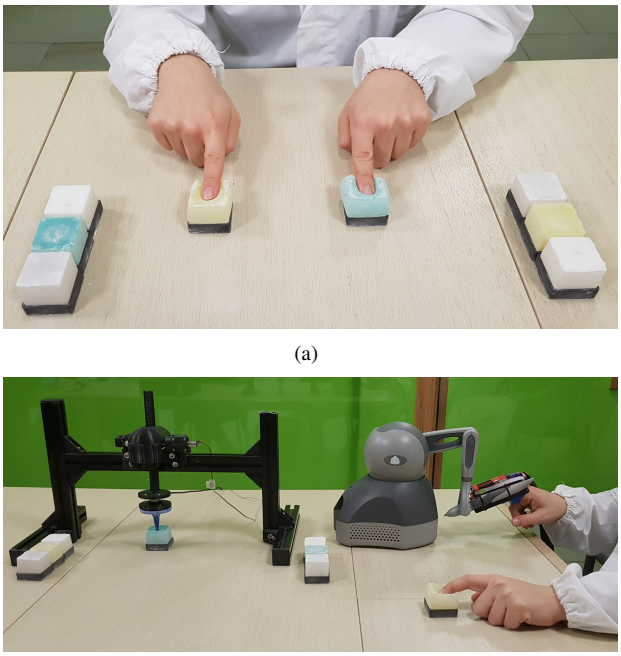

(a)

(b)

Fig. 1. Experimental setup (a) Ground Truth Condition (b) Evaluating Condition. In (b) it is also possible to observe the architecture with the W-FYD system worn by a surgeon and fixed to the teloperating console, i.e. a Geomagic Touch stylus.

However, the precise localization of myomas still represents a challenging part, despite the improvements of the ecographic techniques [7]. Indeed, the incorrect identification of the fibroid could come with a precautionary, yet often unnecessary, removal of a large part of the uterine tissues. This condition is specifically negative for fertile women. On the contrary, making the surgeon aware of the position of the myomas through specific haptic feedback - which should ideally be close to the touch-related information that would be naturally gathered during direct, physical palpation [8] - could enable the precise localization of the fibroids and hence their removal, minimizing the impact and damages to the other tissues of the uterus.

II. State of the art

In literature we can find several haptic devices, both kinaesthetic and cutaneous, which were specifically designed for lump localization, targeting laparoscopic and robotics-enabled surgery. Kinesthetic solutions [9]–[12] have to deal

This project has received funding from the European Union's Horizon 2020 research and innovation programme under grant agreement No. 871237 (Sophia) and grant agreement No. 732737 (ILIAD), and by the Italian Ministry of Education and Research (MIUR) in the framework of the CrossLab project (Departments of Excellence). The content of this publication is the sole responsibility of the authors. The European Commission or its services cannot be held responsible for any use that may be made of the information it contains.

[†] Centro di ricerca E. Piaggio, University of Pisa, Pisa PI 56122, Italy

[††] Division of Obstetrics and Gynecology, Department of Clinical and Experimental Medicine, University of Pisa, Via Roma, 67, 56126 Pisa, Italy

[‡‡] Information Engineering Department, University of Pisa, Pisa PI 56122, Italy

[1] https://intuitivesurgical.com/

with stability issues that may affect the teleoperation loop, arising when grounded forces are output with the teleoperating console [13]. A preferable approach for stability is *sensory substitution*, where the cutaneous component of haptic feedback is conveyed to the user without the kinaesthetic one [14], making the teleoperation system intrinsically stable. At the same time, cutaneous feedback can be more easily implemented in robotic surgery, since it does not require to significantly modify the teleoperating interface. Furthermore, cutaneous cues were proven to be more informative than kinaesthetic ones in softness discrimination tasks [15], [16], like the one that surgeons usually perform to detect hard nodules embedded in the tissues.

State of the art cutaneous lump devices include "pin-array" tactile displays [17]; air-jet and pneumatic displays [8], [18], [19]; granular and particle jamming displays [20], [21]; magnetorheological fluid haptic displays [22]. However, these solutions could face important challenges when they come to be implemented in teleoperation architectures (which are related to size and dimension constraints and to the need for ensuring an unobtrusive interaction with the surgeons, as discussed in [8]) and were not tested in teleoperation tasks with real end users.

In [14], the authors compared four cutaneous displays for pinching palpation in robotic surgery. More specifically a tilting plate display; a rigid platform display; a variable compliance platform display; a band and linkage display. Results showed that the variable compliance platform, inspired by [23], performed better than the other ones, for rendering soft and medium-hard materials. However, these solutions were not tested in teleoperation procedures with surgeons.

Importantly, none of the aforementioned devices was specifically designed for, and tested in, gynecologic RMIS applications, where the absence of haptic feedback in RMIS procedures represents a well-documented cause of incomplete removal of myomas and of higher incidence of recurrent myomas [24].

Motivated by these observations and by the outcomes in [14], in this work we propose to integrate the wearable version of [23], the W-FYD, in a teleoperation architecture that simulates a robot-assisted surgical palpation of leiomyomas, see Figure 1(b), and to test the system with 13 gynecologic surgeons. The W-FYD consists of a fabric whose stretching state can be modulated by controlling two DC motors, to which the fabric is attached (see Section III-B). In this manner, different softness characteristics can be reproduced. We chose to use a wearable interface, although fixed to the teleoperating console, to enable the surgeons to unobtrusively interact with the device during palpation procedures.

One important contribution of our work was the *ex-vivo* characterization of the uterine tissues, to show the effectiveness of our interface in delivering meaningful softness information. To this aim, we determined the stiffness workspace of uterine tissues with embedded fibroids. Furthermore, to demonstrate the effectiveness of the usage of the W-FYD, we involved gynecologic surgeons in the evaluation of our integrated teleoperation system, in a simulated RMIS palpation task with silicone specimens. The latter were designed to reproduce the characteristics of uterine tissues with embedded leiomyomas.

In [25], we anticipated the possibility to use the feedback provided by W-FYD in gynecologic robotic surgery for myoma localization. However, we did not perform a mathematical characterization of the uterine samples, which drove us to devise the control law for the W-FYD. Furthermore, we did not develop the integrated teleoperation, and we did not test it with real end users. In this paper, we present the teleoperation system for palpation tasks, where we integrated the W-FYD. We also report a quantitative *ex-vivo* characterization of uterine tissues and the experimental evaluation of the system with medical residents in the Gynecologic Clinics of the Pisa Hospital. The experimental procedure was approved by the Ethical Committee of the University of Pisa (Number 1072/2016 CEAVNO).

III. The System

We designed a teleoperation system, which can indent an object (more specifically a biolgical tissue or a silicone specimen) and compute the indentation amplitude and the force applied on it, to retrieve its stiffness characteristics. The teleoperation system was composed by two main components, the console, or teleoperating part, and the teleoperated part, or *Indenting System* .
In this work, we fixed the Wearable Fabric Yielding Display (W-FYD) [26] to the teleoperating device. The objective was to unobtrusively convey softness information on the specimen indented by the teleoperated system to the human operator, while he/she was controlling the console to perform a task that simulated surgical myoma palpation. In the following, we report the main components of our architecture.

A. The Indenting System

The *Indenting System* (see Figure 2(a)) is a two Degrees of Freedom (DoFs) mechatronic device, which can perform a controlled indentation on an object (in our work we considered fibromatosis uterine tissues and silicone specimens), while gathering force and displacement information. The system can be controlled via PC or can act as a teleoperated device (see later in this section). In the former case, it is used to characterize the stiffness workspace of a probed object as in [23].

The structure of the *Indenting System* was realized in ABS 3D printing material. It is endowed with two DC motors DCX 10L with a 256:1 gearmotors GPX 10 (Maxon Motor, Sachseln, Switzerland)[2], and consists of three main parts: (1) the *indenter* (in blue in Figure 2(a)), a pinion and rack system that allows to press the specimen surface along the vertical direction; (2) the *rotary base* (in Yellow in Figure 2(a)), which allows to vary the indentation angle α of the *indenter* (α equal to zero means that the *indenter* is perpendicular to the *frame*, see below and Figure 2(a)), to guarantee an indentation direction parallel to the inward normal direction of the surface under exploration, moreover, it hosts the DC motor

[2]https://www.maxonmotor.com

that actuates the *indenter*; (3) the *frame* (in red in Figure 2(a)), which contains the second DC motor that actuates the *rotary base*, and a fixing system. The latter allows to fix the overall *Indenting System* to an external grounded frame. To measure the pinion angle γ, we placed a magnetic encoder AS5045 (asm AG., Shanghai)[3] with $0.0879°/step$ resolution at the head of the shaft of the DC Motor that actuates the *indenter*. With this structure, it is possible to compute the indentation δ produced on the explored specimen as $\delta = R\gamma$, where R is the pinion radius. The force exerted on the specimen by the *indenter* can be measured through an ATI Nano17 (ATI Industrial Automation Inc., USA)[4] with 16 bit resolution, which was placed on the rack (see Figure 2(a)).

When used to characterize the stiffness workspace of a specimen as in [23], the *Indenting System* was connected to a PC through a USB cable. A custom-made software written in C++ was used to control the indentation of the system based on the equation $\delta = R\gamma$ and on the selected indentation velocity. The stiffness characterization of a specimen consists of an initialization phase and an acquisition phase. At the beginning of the initialization phase, the software required to provide the desired indentation angle for α and to choose the indentation velocity, between $v_1 = 3.2mm/s$ and $v_2 = 48.27mm/s$. These velocities were chosen according to the study [27], which analyzed the relation between the indentation velocity and the detection rate of salient features during soft tissue examination. During the acquisition phase, the *indenter* moved vertically to probe the specimen, while force and γ values were collected through the force/torque sensor and the magnetic encoder, respectively. Data acquisition was managed using the NetBox for the ATI Nano17 - force and torque information - and the qbrobotics board interface (Natural Machine Motion Initiative)[5] for the AS5045 encoder. The communication between these control interfaces was implemented at a frequency of $1.8kHz$. The stiffness coefficient K was computed at each clock cycle as the ratio of the force value F and δ ($\delta = R\gamma$). A PID controller, which was implemented on the qbrobotics board, was tuned for the control of the motor that actuates the *indenter*, to guarantee a null velocity error (another PID controller was set for the position control of the DC motor of the *rotatory frame*). The entire *Indenting System* was powered through a 12V battery.

The *Indenting system* also acted as a teleoperated device to be used in palpation tasks, which received position commands from the teleoperating console, i.e. a mid-range professional haptic device, the Geomagic Touch[6] (3D System, USA). In this work, we fixed the W-FYD to the stylus of the Geomagic Touch, to convey softness information - computed from the force and indentation information acquired through the *Indenting System* - to the human operator (see also Section V-B1). In Figure 1(b) we show the W-FYD system worn by a surgeon and connected to the teloperating console. The connector was realized in ABS-printed material and designed to not hamper the movements of the Geomacic Touch device and those of the user.

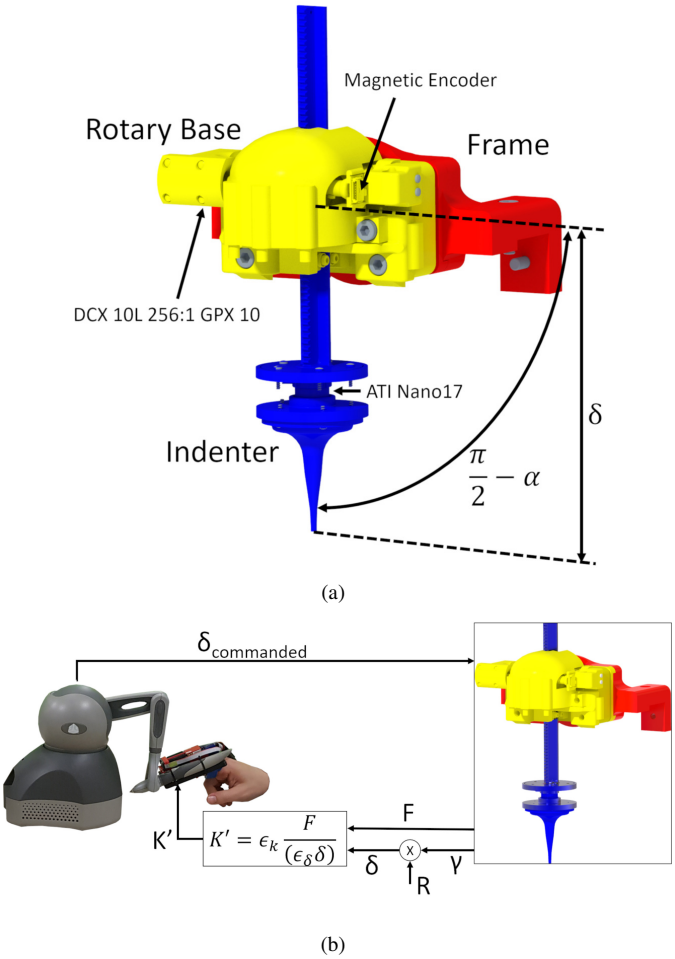

Fig. 2. Indenter system CAD design (a). The indenting part is in blue, the rotary base in yellow and the frame in red. In (b) the control scheme of the teleoperated system is reported. In the figure, α is the indentation angle, δ is the indentation (see section III-A), F is the instantaneous measured force, R and γ are the radius and the instantaneous measured angle of the pinion (not visible, positioned inside the Rotary Base structure), ϵ_δ and ϵ_k are the scaling coefficients respectively for indentation and stiffness, K' is the computed stiffness, $\delta_{\text{commanded}}$ is the position command sent from the teleoperating console to the Indenting System. See Section IV-C for more details.

When the *Indenting system* was employed in the teleoperation configuration, only the vertical indentation ($\alpha = 0$) was used. This was done to avoid the application of lateral forces that could provoke anisotropic or distortion effects that could affect the softness perception elicited through the wearable device [23], [28].

It is important to underline that the Geomatic touch was used as input device only, and no-force feedback was provided through the same device to the user. The tactile feedback was delivered through the W-FYD, which was controlled in the *passive mode*, see Section III-B. In this way, we decoupled the input command from the feedback information allowing the loop to be intrinsically stable.

More specifically, the user wore the W-FYD on the index finger of the right hand and performed a vertical movement with the wrist, which involved the whole hand, without flexing the finger. Since the W-FYD was rigidly connected to the stylus

[3]https://asm.com
[4]https://www.ati-ia.com
[5]https://www.naturalmachinemotioninitiative.com.
[6]https://it.3dsystems.com/haptics-devices/touch

of the Geomagic Touch, the user's movement was reflected in the movement of the end-effector of the Geomagic Touch itself. Relying on inverse kinematics algorithms, the movement of the joints of the Geomagic Touch was then translated in the commanded δ to be transmitted to the *Indenting system* [29]. In this manner, the teleoperated device performed an active indentation of the sample, which was placed below the *indenter*.

The sample stiffness was computed at each instant relying on the force and indentation information, which was gathered through the *Indenting system* as described before, through a custom-made C++ software. The same software was also in charge of controlling the W-FYD to deliver meaningful softness information on the user's fingertip (described in Section V-B). See Figure 2(b) for the control scheme of the teleoperation loop.

The communication between the teleoperated system and the sensor control interfaces (NetBox and qbrobotics board) was implemented at a frequency of $25Hz$. This means that the stiffness was computed from force and indentation data and sent as reference input to the W-FYD every 40 ms.

B. W-FYD: Wearable Fabric Yielding Display

The W-FYD, a wearable fabric-based haptic device [26] [30], is a tactile display that can convey controllable softness information to the user's finger-pad, by regulating the stretching state of a fabric band through two DC motors. It allows both *active* and *passive* haptic exploration. The device can be placed over the user's finger, and fixed to it with an elastic clip that prevents rotation and ensures stability. It consists of two parts: the base, which is fixed and equipped with a lifting mechanism; and the frame, which hosts the two DC motors that independently move two rollers to which the elastic fabric is attached, thus varying its stiffness. Two pins are connected to the frame through supports, which ensure a planar interaction surface of the fabric.

In the *active mode*, which is used to enable an active surface exploration, the user can perform the flexion of the distal phalanx of the finger; the resulting movement of the fingertip is measured through an infra-red sensor and used to control the two DC motors and hence the fabric stretching state, to reproduce a given stiffness profile. In the *passive mode*, an additional vertical degree of freedom is implemented through a lifting mechanism, which moves the entire frame with respect to the base. The lifting system allows to push the fabric against the user's finger, which is still, while the softness information is rendered by regulating the stretching state through the two DC motors. Since the fabric stretching is actuated separately from the lifting mechanism, the stiffness of the fabric can be changed independently and is decoupled from the force exerted on the user in the passive mode. The passive mode was used for the experiments reported in this work. For more details on the W-FYD device, please refer to [26], [30].

IV. System Characterization

The leading idea of this work is the usage of the softness feedback delivered through the W-FYD for enhancing the localization of uterine leiomyomas. To this aim, it is important to define the clinical requirements, i.e. which is the stiffness of the fibrotic tissue and the one of uterine tissues without any myomas, and whether it is possible to use the W-FYD to replicate these stiffness characteristics, eventually relying on a suitable scaling coefficient. In this section, we report the results of the *ex-vivo* characterization of uterine tissues with embedded myomas and those of the silicone specimens we used in our experiments with human participants. We comparatively discussed these outcomes, also with respect the stiffness workspace that our wearable interface can reproduce.

A. Ex-vivo Sample Characterization

For the *ex-vivo* sample characterization, we considered two fibromatosis uteri, hereinafter referred to as U1 and U2 (patient age: 68 and 73 years respectively - see Figure 4). Different areas of interest for data acquisition were identified on the uteri by the surgeons. The selected areas were: body left (U1BL and U2BL), body right (U1BR and U2BR), isthmus left (U1IL and U2IL) and isthmus right (U1IR; U2IR) for a better representation of the different areas.

In the rest of the paper, the fibroids in the area of interest are indicated with specific suffixes: "_SF" refers to a subserous fibroid, "_I" refers to an intramural fibroid. The uterine tissues without fibroids are named with the suffix "_free".

U1 contained two subserous fibroids, one in the area U1BL (U1BL_SF) and one in the area U1BR (U1BR_SF), and an intramural fibroid in the area U1BR (U1BR_I). The latter was located within the muscular wall of the uterus. U2 contained two subserous fibroids, one in the area U2BL (U2BL_SF) and one in the area U2BR (U2BR_SF), see Figure 3.

We characterized the stiffness of the different uterine areas, using the *Indenting system* controlled via PC, as described in Section III-A. We performed different acquisitions on each area shown in Figure 3, varying the indentation angle (range of ± 45 degrees) and the indentation velocity ($v_1 = 3.2mm/s$ and $v_2 = 48.27mm/s$). The indentation angle was changed to guarantee an indentation direction parallel to the inward normal direction of the surface under exploration (see Figures 4(a) and 4(b)). We performed five acquisitions on each area, for a total of 150 acquisitions per uterus.

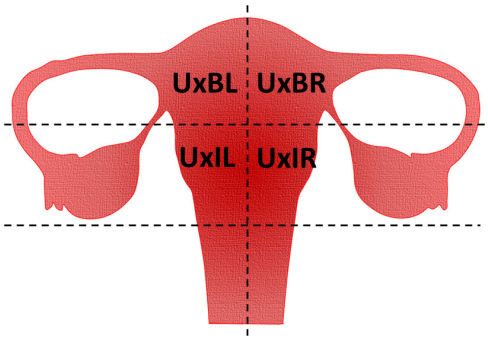

Fig. 3. Illustration of the uterus and visualization of the areas we considered for data acquisition. The labels UxBL and UxBR refer to Uterus x, Body Left and Right, respectively; UxIL and UxIR refert to Uterus x, Isthmus Left and Right, respectively.

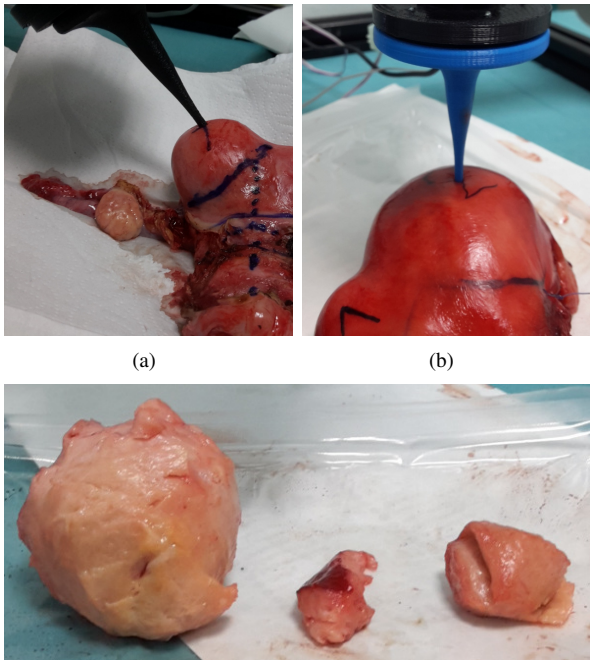

(a) (b)

(c)

Fig. 4. The top figures show two examples of data acquisition from the two tested uteri, U1 and U2: (a) characterization of U1 with an indentation angle $\alpha = 45$ deg; (b) characterization of U2 with an indentation angle $\alpha = 0$ deg. In (c) the extracted samples are presented. In the center, the 15 mm edge cubic shape piece of uterine tissue is shown. On the left the U2BR_SF fibroid with diameter 60 mm; on the right the elliptic shaped fibroid U2BL_SF with dimensions 30x20 mm. Reprinted by permission from Springer-Verlag London Ltd., part of Springer Nature: Springer Nature, Journal of Robotic Surgery, [25], ©2019

We also extracted a cubic sample (15 mm edges) of uterine tissue from U2BL (from now on referred as U2_tissue); the two subserous fibroids U2BL_SF and U2BR_SF were also extracted, to directly characterize their stiffness, without any interference from the surrounding tissues (Figure 4(c)). For these samples, the measures were collected with a vertical indentation (α equal to zero deg), performing five acquisitions for each indenting velocity.

We found negligible differences in the stiffness characteristics obtained for the two velocities, as we can see in the exemplary plots reported in Figure 5 (force/indentation characterization for the U1IR_free).

For each tested sample, we computed the force/indentation characteristics interpolating the data using a second order polynomial curve. The raw data together with the interpolated curves are reported in Figure 6. Figure 6(a) shows the results for U1: U1BL, U1BR, U1IL and U1IR; Figure 6(b) shows the results for the samples removed from U2: the two subserous fibroids, U2BL_SF and U2BR_SF, and the sample of uterine tissue U2_tissue. Since we found no differences in the characterization curves considering the two velocity bounds, for the sake of readability we report only the data obtained using as indentation velocity $v_1 = 3.2mm/s$.

B. The Silicone Samples

To perform an extensive evaluation of our system in teleoperation tasks, we designed a set of silicone samples, whose

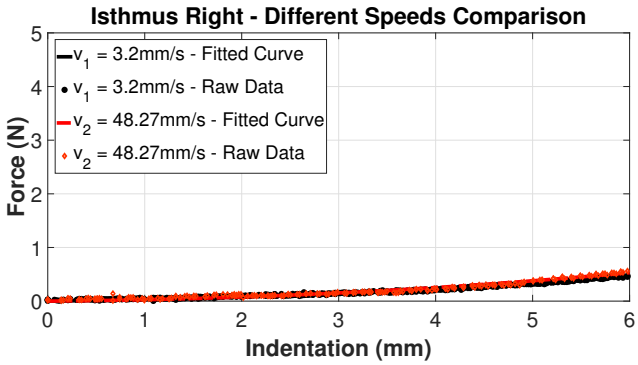

Fig. 5. Force/Indentation characterization of U1IR. The figure shows the raw data for the two velocities $v_1 = 3.2mm/s$ and $v_2 = 48.27mm/s$, and the interpolated curves (second order polynomial fitting, adjusted R^2 equal to 0.9893 for v_1 and 0.9661 for v_2).

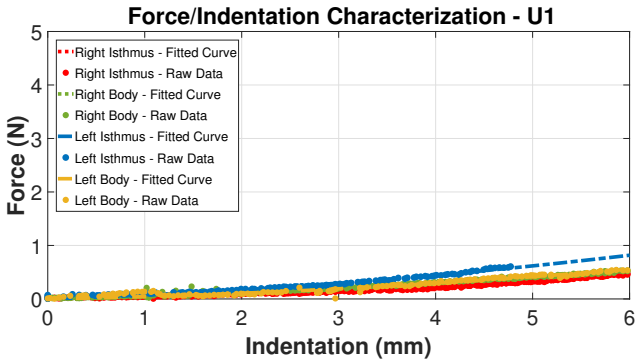

(a)

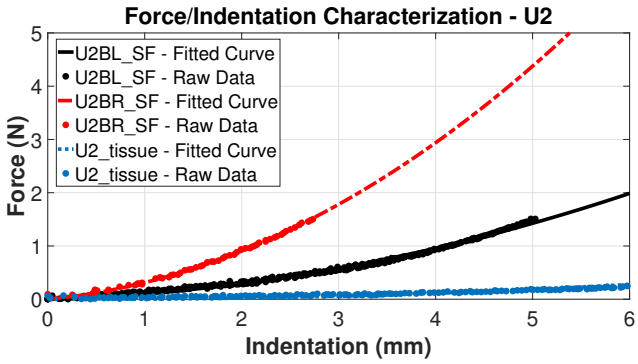

(b)

Fig. 6. Force/Indentation characterization: raw data and interpolation curves (second order polynomial fitting, adjusted R^2 always greater than 0.9592). These data were obtained with an indentation velocity $v1 = 3.2mm/s$, taking measurements from U1BL, U1BR, U1IL, U1IR and U1BR_I (a), U2BL_SF, U2BR_SF and U2_tissue (b).

stiffness characteristics were close to the ones of the uterine tissues. These samples were composed of two parts (see Figure 7(a)): the *lump* was molded with Sylgar 184 (downcorning, USA) to simulate a subserous fibroid, in the shape of a sphere with a 6.5 mm diameter (this dimension is in agreement with [31], [32]); a *cube* molded with Ecoflex 00-30 and Slacker (Smooth-on, USA)[7] in 1:1:3 ratio was used to simulate U2_tissue. We created a total of four samples:

[7]https://www.smooth-on.com

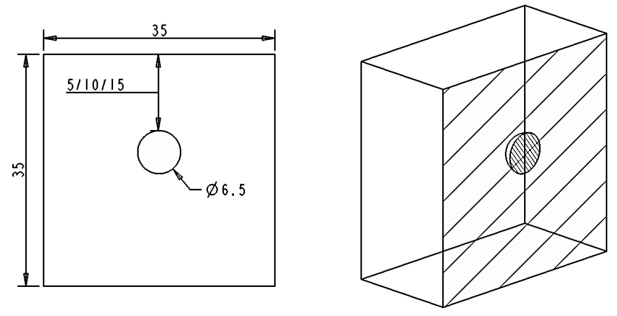

(a)

(b)

Fig. 7. Physical description of a section of the silicone model (a). A cubic shape of 35mm molded with Ecoflex 00-30 and Slacker in 1:1:3 ratio and a spherical shape with 6.5mm diameter molded with Sylgar 184 in three different depth (b), respectively 5mm (white), 10mm (yellow) and 15mm (green). There is an additional sample with any lump (transparent). The measurements in the figure are in mm.

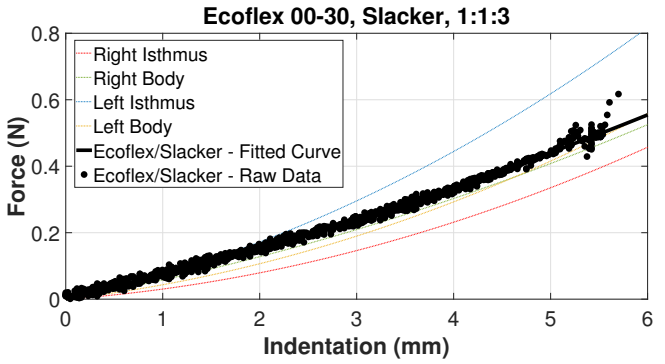

(a)

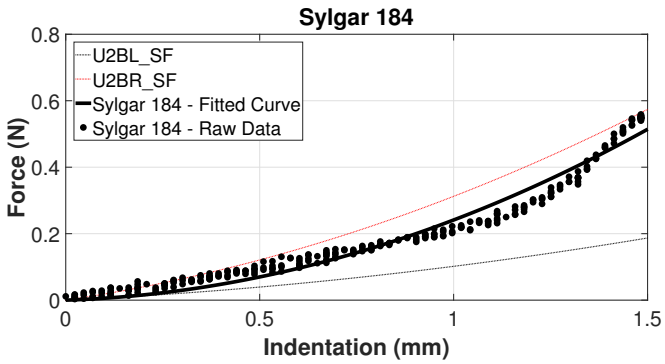

(b)

Fig. 8. Force/Indentation characterization for the components of the silicone samples: raw data and interpolation curves (second order polynomial fitting, adjusted R^2 always greater than 0.9701). These data were obtained with an indentation velocity $v1 = 3.2mm/s$ from measurements on the Ecoflex 00-30, Slacker, 1:1:3 sample of cubic shape of 35mm (a) and the Sylgar 184 sample of spherical shape with 6.5mm diameter (b), in comparison with real samples showed in Figure 6.

three with different depth of the *artificial fibroid*, 5mm, 10mm and 15mm, and one without fibroid (see Figure 7(b)). These depth values were chosen based on the clinical practice of the surgeons involved in our study, to cover the most common clinical situations, without any claim of exhaustiveness. Under this regard, it is also worth considering that the thickness of the uterus is around 3 cm [1], [2]. A careful investigation of the depth threshold beyond which myomas cannot be reliably localized is out of the scope of the current work, and it will deserve future clinical studies.

As we did for the *ex-vivo* samples, we characterized the stiffness of the silicone samples performing five measurements per sample ($\alpha = 0$ and indenting velocity of $v1 = 3.2mm/s$).

In Figure 8 we report the raw force and indentation data and the fitted ones (polynomial second order fitting, adjusted R^2 always greater than 0.9701), together with the data related to the biological counterparts. It is possible to observe that the stiffness of the silicone cube is within the range of the uterine samples (see Figure 8(a)). We can also observe the similarity between the stiffness of the fibroids U2BL_SF and U2BR_SF, with the hard silicone lump embedded in the artificial samples (see Figure 8(b)).

C. The Stiffness Rendering

The silicone specimens were used in the experiments with gynecologic surgeons, in a palpation task performed with the teleoperation architecture described in Section III-A. The *Indenting system*, which received position commands by the surgeon while using the teleoperating console, pressed the silicone specimen. At each clock cycle (i.e. every 40 ms), the force and indentation data were gathered and used to compute an instantaneous stiffness coefficient, which was sent to W-FYD. In this manner, the stiffness characteristics of the silicone specimens were reproduced using the W-FYD controlled in the *passive mode*. The force and indentation measurements were scaled as

$$\delta' = \epsilon_\delta \delta \tag{1}$$

$$K' = \epsilon_k \frac{F}{\delta'} \tag{2}$$

Where ϵ_δ is the indentation scaling coefficient, ϵ_K is the stiffness scaling coefficient, δ' is the scaled indentation used to control the lifting mechanism of the W-FYD system and K' is the computed stiffness used for the motors angles $\theta_2 = -\theta_1 = \theta$ computation with

$$\theta = 16.25e^{5.024K'} - 2.232 \cdot 10^{-4} e^{-30.63K'} \tag{3}$$

This equation was obtained from the data of the W-FYD characterization performed in [26].

The indentation scaling coefficient was computed to allow to put in correspondence the maximum indentation in the silicone specimens (3.5 cm) and the maximum height achievable by the lifting mechanism of the W-FYD (1.5 cm).

The stiffness range that W-FYD can reproduce is between 0.15 to 0.35 N/mm. The stiffness scaling coefficient was used

to align the minimum and maximum value of the silicone stiffness to the span reproducible by W-FYD. Looking at the characterization data for the two components of the silicone specimens, we found a maximum stiffness of 0.38 N/mm and a minimum stiffness of 0.07 N/mm; those values were used for the stiffness scaling coefficient computation.

V. Experiment

The goal of this experimental session consisted in the evaluation of the capability of the users to discriminate the presence of leimyomas in terms of softness stimuli in an absolute recognition task, with silicone specimens. The stimuli were rendered in real-time on the user's finger-pad through the W-FYD.

A. Participants

Thirteen participants (5 Female, Age mean±SD: (29.77±3.22), of which twelve medical residents and one senior experienced clinician, took part to the study. No one had any physical limitation which would have affected the experimental outcomes. They gave their informed consent to participate to the experiments.

B. Task

The task of the experiment consists in the evaluation of the user capability in discriminating the presence of the myomas using stiffness tactile feedback in real-time in two different conditions. The first condition, named the *Ground Truth Condition*, consisted in the discrimination of the lump in the silicone samples without the use of the system, but relying on direct palpation. In the second condition, named *Evaluating Condition*, the surgeons were required to perform the same task using the teleoperation architecture with the W-FYD.

The two conditions were presented in random order within participants.

1) Ground Truth Condition: The participant was sitting in front of the table, wearing a pair of googles with opaque lenses, to avoid any visual cue (see Figure 1(a)).
A total of 40 random trials were presented to the user (10 times for each sample). For each trial, the test sample was placed below the index finger of the user's right hand and the participant was asked to performs some exploration on it. At the same time, the user was allowed to perform an exploration with the left hand index finger on all the four comparison samples, one at the time and in the same order for each trial, and was asked to identify which of these corresponded to the test sample.

2) Evaluating Condition: The participant was sitting in front of the table, wearing the W-FYD system on his right hand index finger; the W-FYD was used in the *passive* mode (as explained in Section IV-C) and attached to the stylus of the Geomagic Touch Device. In addition the participants wore headphones with pink noise and a pair of goggles with opaque lenses, to avoid any auditory and visual cue (see Figure 1(b)).

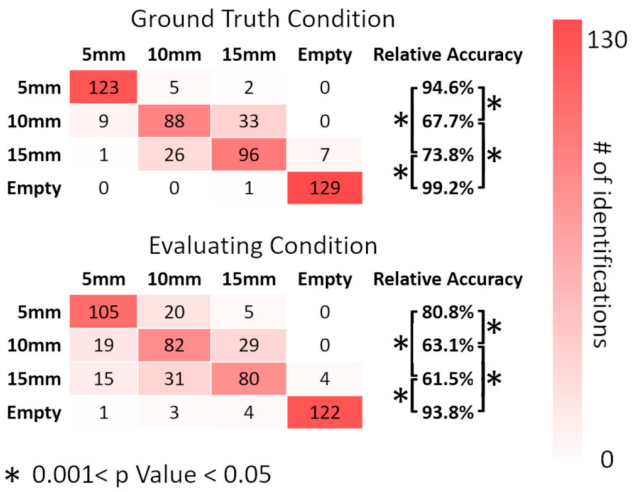

Fig. 9. Confusion Matrices with the experimental outcomes.

At the beginning of the task, we put a silicone sample under the *Indenting system*. The user was able to control the indenter motion through the Geomagic Touch Device only along the vertical direction.
A total of 40 random trial were presented to the user (10 times for each sample). For each trial, the test sample was placed below the *indenter*. The user was asked to perform a tele-exploration with the index finger of the right hand, while (s)he was wearing the W-FYD. The user was free to choose the indentation velocity: at the beginning of the trial (s)he was instructed to stay in the range of velocities between v_1 and v_2. At the same time, the user performed an exploration with the index finger of the left hand, preferably with the same velocity of the right hand, on all the four comparison samples, one at the time, in the same order for each test, and was asked to identify which of these corresponded to the test sample.

At the end of the experiment, the participants underwent through a subjective quantitative evaluation test using a seven-point Likert-type scale (1: Strongly disagree, 7: Strongly agree), as in [26], [33], [34].

VI. Results

Results of the *Experiments* are presented through two confusion matrices reported in Figure 9, one for each condition, with the relative accuracy in discrimination for each specimen. The correct answer of all tests are reported in the diagonal of these matrices. The results of the *Ground Truth Condition* are shows in the upper part of Figure 9. The average of relative accuracy for the ground truth rate is 83,8%±15,4% (mean±SD), with chance level of 25%.

The results of the *Evaluating Condition*, instead, are shows in the lower part of Figure 9. The average of relative accuracy for the Evaluating rate is 74,8%±15,4% (mean±SD), with chance level of 25%.

A Friedman test was used to compare the Evaluating Condition and the Ground Truth Condition results considering four repeated measures for each subject (one for each experimental condition of the position of myomas, i.e. depth of 5 mm,

10 mm, 15 mm, and no myoma). No statistical difference was found ($p > 0.05$) between the two conditions. This means that there are no statistical differences between subjects' performances while interacting directly with the samples and while interacting through the presented device.

Furthermore, we performed four Wicoxon signed rank tests between the scores obtained with the device and in the ground truth condition referred to each experimental depth of the simulated fibroid. In post-hoc analysis, we compared the scores of each singular experimental session, using a two-tailed Wilcoxon signed-rank test with false discovery rate (FDR) adjustment through the Benjamini-Yekuteli correction. The analyses revealed statistically significant differences between the depth conditions 5 mm vs. 10 mm ($p = 0.002$ ground truth, $p = 0.017$ device), 5 mm vs 15 mm ($p = 0.001$ ground truth, $p = 0.037$ device), 10 mm vs empty and 15 mm vs empty ($p = 0.005$ ground truth, $p = 0.002$ device), for both the ground truth and the device session. There are no statistically significant differences between 10 mm and 15 mm and 5 mm and the empty condition: these results hold both in the *Ground truth condition* and the *Evaluating condition*, and cannot be regarded as a limitation of our device.

In Table I the result of the quantitative evaluation are reported. The participants answers with a value of 1 mean totally disagree and 7 totally agree. Results show that participants perceived the tactile feedback from W-FYD intuitive and easy to distinguish within the different stimuli (Q1, Q3, Q6). Furthermore participants agree on the utility of the integration of the W-FYD with the tele-presence robotic system in laparoscopic robotic myomectomy (Q5, Q7).

VII. Discussions and Next Steps

A. Discussions

In this paper, we present a teleoperation architecture with integrated softness feedback, which was designed to perform palpation tasks. To the best of authors' knowledge, this is the first paper that specifically targets the delivery of cutaneous information for RMIS gynecologic applications (detection of uterine fibroids). To this aim, we moved from an *ex-vivo* stiffness characterization of the uterine tissues and fibroids. This enabled us to develop silicone samples with similar characteristics with respect to biological samples, in terms of force and indentation information, which were used in the experimental validation with surgeons, and to check the effectiveness of the usage of the wearable device [26] in conveying meaningful softness information. By comparatively analyzing the stiffness workspace that can be reproduced using the W-FYD and the one of the silicone specimens (which can be regarded as reliable approximations of the biological samples), we identified a suitable scaling coefficient to align the minimum and maximum value of the silicone stiffness to the span reproducible by the wearable fabric-based device.

We tested our teleoperation architecture in palpation tasks performed by medical residents of the Gynecologic Clinics of the Pisa Hospital. This represents another important contribution of our work. Indeed, we do believe that a successful integration of tactile feedback in RMIS procedures should undergo through the assessment of real end users. Experimental outcomes show that there are no statistical differences in participants' performance (i.e. discrimination accuracy of silicone specimens with embedded lumps at different depth values), considering the two cases, i.e. direct sample palpation with the finger and sample exploration using the teleoperation system with the integrated tactile feedback. This result opens to promising perspectives in gynecologic RMIS, where the lack of informative tactile and haptic cues represents a well-documented cause of incomplete removal of myomas and of higher incidence of recurrent myomas [24]. Looking at the results of the subjective quantitative evaluation, the tactile feedback was evaluated as intuitive, comfortable and effective. This suggests that the softness information delivered through the W-FYD could be an important factor to improve the localization of uterine fibroids in surgical procedures. It is important to underline that we used a wearable device, but it was fixed to the teleoperating console. The choice of a wearable system was motivated by the need for enhancing the comfort of the surgeons while they were interacting with the feedback device. The scores provided by participants to questions Q4 and Q2 in Table I confirm that the usage of our tactile system did not hamper the surgeons and was not uncomfortable.

B. Envisioned flowchart for an effective integration in RMIS systems and next steps

Of note, despite the positive outcomes, the flowchart leading to an effective integration of our cutaneous display in existing RMIS systems should face important challenges and undergo through several intermediate steps. First, additional tests with our teleoperation architecture are needed, before moving to real clinical scenarios, considering more experimental conditions (e.g. different lump sizes), a larger pool of participants, and the usage of a fully wearable version of the tactile device. Under this regard, the wearability of our cutaneous system should be further improved. In this manner, the W-FYD could be easily used with several FDA-approved RMIS platforms [35]. Indeed, it could be worn by the surgeon, while using the adjustable finger loops of the teleoperating robot of the Da Vinci Surgical system [36]. Interestingly, since the interaction surface of the W-FYD is a fabric, it does not impair the natural cutaneous perception on the users' finger (as discussed in [26] for what concerns the paradigm of tactile augmented reality), thus opening to its usage also with other FDA-approved RMIS systems, such as the Senhance system [12]. This system uses a parallel kinesthetic force feedback haptic device as teleoperating robot. With the W-FYD, the surgeon could still handle the teleoperating haptic interface with her/his hand, without any limitation to her/his tactile sensitivity, while receiving informative tactile cues through on the finger, e.g. within the general framework of *sensory subtraction* - to further increase transparency without compromising stability [13].

The integration of our cutaneous display in a robot-assisted minimally invasive surgery platform should also require the development of suitable sensing strategies for the teleoperated robot, for retrieving tissue stiffness information. In

TABLE I
7-POINT LIKERT-SCALE.

	Question	Median	IQR	CI m. 95%
Q1	The feedback provided through the W-FYD is intuitive.	5	1	5.6
Q2	I was feeling uncomfortable while using the W-FYD.	3	3	2.4
Q3	When present, the fibroma is easy to perceive using the W-FYD.	6	2	5.7
Q4	I felt hampered by the W-FYD.	3	2.5	3.4
Q5	The integration of haptic device with the tele-presence robotic system is useful for the recognition of the presence of myomas during laparoscopic robotic myomectomy.	6	1	6.7
Q6	It is difficult to distinguish the indentation stimulus from the stiffness information.	2	3.5	2.3
Q7	The integration of the W-FYD ith the tele-presence robotic system is useful for the high-precision localization of the myoma during laparoscopic robotic myomectomy.	6	2	5.6

the approach reported in this work, this was obtained by relying on both force and indentation sensing. However, an effective translation of this solution in real scenarios is not straightforward and comes with important challenges, which are related to the millimeter-scale size of medical instruments and sterilization, among the others [37], [38]. The measurement of the interaction forces [39] can be achieved through sensor-based methods, contact-less methods and force estimation, with promising results – see [37] for a review on these topics. Of note, a reliable measurement of organ indentation is more challenging, e.g. due to the nonlinear and variable characteristics of soft tissues. A possible way to overcome these limitations could be to rely on the usage of tactile sensors: under this regard, it is worth mentioning piezoelectric elements for a direct tissue stiffness sensing [40], or piezoresistive and capacitive sensor arrays, which were engineered in low-cost, sterilizable versions with minimal wires [41]. Another approach could be the application of soft electronic sensors, which were demonstrated to be a promising solution for clinical practices of palpation [42].

It is also worth noticing that the direction of exploration influences the discrimination of softness. For these reasons, in our experiments we constrained the exploration along the normal direction to the surface, as done also in [43], preventing movements across the surface and the application of lateral forces. This allows avoiding any anisotropic or distortion effect in softness perception [28]. However, in real applications, the approach angle of the teleoperated robot with respect to the surface normal could be different from zero and other physical properties of the samples could influence the perception, e.g. superficial friction. This aspect will deserve specific attention as future work, while tackling the translation of our outcomes in clinical settings. Under this regard, we will consider implementing an independent control of the two motors of the haptic display, to enable an anisotropic control of the stretching state of the fabric. At the same time, we will also evaluate the superposition of high frequency information to reproduce the frictional and roughness properties of the samples under exploration, as we did in [44]. Finally, it is worth noticing that the speed of palpation represents a key factor that influences the detection rate of hard nodules as reported in [45]. Lower exploration velocities are associated to higher accuracy discrimination levels. The working frequency of the system is fully compatible with the velocity range in [45], although it relates to the communication-control loop of the teleoperation system. It is important to underline that the device is currently controlled in position. A velocity control will be explored in future work, which could be also used to reproduce dumping effects of the fibromatosis uterus, eventually estimated relying on the techniques in [46].

ACKNOWLEDGMENT

The authors would like to thank Francesca Montemurro for her help in building the silicone specimens; Mimma Nardelli for her suggestions on how to perform the statistical analyses and all the medical residents of the Gynecologic Clinics of the Pisa Hospital, who were involved in our experiments.

REFERENCES

[1] E. C. Klatt, *Robbins and Cotran atlas of pathology*. Elsevier Health Sciences, 2014.

[2] E. A. Stewart, S. K. Laughlin-Tommaso, W. H. Catherino, S. Lalitkumar, D. Gupta, and B. Vollenhoven, "Uterine fibroids," *Nature Reviews Disease Primers*, vol. 2, no. 1, pp. 1–18, jun 2016.

[3] E. A. Stewart, "Uterine fibroids," *New England Journal of Medicine*, vol. 372, no. 17, pp. 1646–1655, apr 2015.

[4] B. HURST, M. MATTHEWS, and P. MARSHBURN, "Laparoscopic myomectomy for symptomatic uterine myomas," *Fertility and Sterility*, vol. 83, no. 1, pp. 1–23, jan 2005.

[5] G. H. Ballantyne and F. Moll, "The da vinci telerobotic surgical system: the virtual operative field and telepresence surgery," *Surgical Clinics*, vol. 83, no. 6, pp. 1293–1304, dec 2003.

[6] E. E. Wallach, V. C. Buttram, and R. C. Reiter, "Uterine leiomyomata: etiology, symptomatology, and management," *Fertility and Sterility*, vol. 36, no. 4, pp. 433–445, oct 1981.

[7] J. Donnez, "Laparoscopic myolysis," *Human Reproduction Update*, vol. 6, no. 6, pp. 609–613, nov 2000.

[8] J. C. Gwilliam, M. Bianchi, L. K. Su, and A. M. Okamura, "Characterization and psychophysical studies of an air-jet lump display," *IEEE Transactions on Haptics*, vol. 6, no. 2, pp. 156–166, apr 2013.

[9] I. E. Rassi and J.-M. E. Rassi, "A review of haptic feedback in tele-operated robotic surgery," *Journal of Medical Engineering & Technology*, vol. 44, no. 5, pp. 247–254, jun 2020, pMID: 32573288. [Online]. Available: https://doi.org/10.1080/03091902.2020.1772391

[10] N. Enayati, E. D. Momi, and G. Ferrigno, "Haptics in robot-assisted surgery: Challenges and benefits," *IEEE Reviews in Biomedical Engineering*, vol. 9, pp. 49–65, 2016.

[11] A. Saracino, A. Deguet, F. Staderini, M. N. Boushaki, F. Cianchi, A. Menciassi, and E. Sinibaldi, "Haptic feedback in the da vinci research kit (dVRK): A user study based on grasping, palpation, and incision tasks," *The International Journal of Medical Robotics and Computer Assisted Surgery*, vol. 15, no. 4, p. e1999, may 2019, e1999 RCS-18-0180.R1. [Online]. Available: https://onlinelibrary.wiley.com/doi/abs/10.1002/rcs.1999

[12] M. Stark, S. Pomati, A. D'Ambrosio, F. Giraudi, and S. Gidaro, "A new telesurgical platform – preliminary clinical results," *Minimally Invasive Therapy & Allied Technologies*, vol. 24, no. 1, pp. 31–36, jan 2015.

[13] D. Prattichizzo, C. Pacchierotti, and G. Rosati, "Cutaneous force feedback as a sensory subtraction technique in haptics," *IEEE Transactions on Haptics*, vol. 5, no. 4, pp. 289–300, 2012.

[14] J. D. Brown, M. Ibrahim, E. D. Z. Chase, C. Pacchierotti, and K. J. Kuchenbecker, "Data-driven comparison of four cutaneous displays for pinching palpation in robotic surgery," in *2016 IEEE Haptics Symposium (HAPTICS)*, IEEE. IEEE, apr 2016, pp. 147–154.

[15] M. A. Srinivasan and R. H. LaMotte, "Tactual discrimination of softness," *Journal of Neurophysiology*, vol. 73, no. 1, pp. 88–101, jan 1995.

[16] E. P. Scilingo, M. Bianchi, G. Grioli, and A. Bicchi, "Rendering softness: Integration of kinesthetic and cutaneous information in a haptic device," *IEEE Transactions on Haptics*, vol. 3, no. 2, pp. 109–118, apr 2010.

[17] M. V. Ottermo, Ø. Stavdahl, and T. A. Johansen, "A remote palpation instrument for laparoscopic surgery: Design and performance," *Minimally Invasive Therapy & Allied Technologies*, vol. 18, no. 5, pp. 259–272, jan 2009.

[18] A. Talhan and S. Jeon, "Pneumatic actuation in haptic-enabled medical simulators: A review," *IEEE Access*, vol. 6, pp. 3184–3200, 2018.

[19] H. Lee, J.-S. Kim, J.-Y. Kim, S. Choi, J.-H. Jun, J.-R. Park, A.-H. Kim, H.-B. Oh, J.-H. Baek, S.-J. Yang, H.-S. Kim, and S.-C. Chung, "Mid-air tactile stimulation using indirect laser radiation," *IEEE Transactions on Haptics*, vol. 9, no. 4, pp. 574–585, oct 2016.

[20] S. Sikander, P. Biswas, P. Kulkarni, B. Atwood, and S.-E. Song, "Prototyping and initial feasibility study of palpation display apparatus using granular jamming," in *2019 IEEE Healthcare Innovations and Point of Care Technologies, (HI-POCT)*, IEEE. IEEE, nov 2019, pp. 71–74.

[21] A. A. Stanley and A. M. Okamura, "Controllable surface haptics via particle jamming and pneumatics," *IEEE Transactions on Haptics*, vol. 8, no. 1, pp. 20–30, jan 2015.

[22] R. Rizzo, A. Musolino, and L. A. Jones, "Shape localization and recognition using a magnetorheological-fluid haptic display," *IEEE Transactions on Haptics*, vol. 11, no. 2, pp. 317–321, apr 2018.

[23] M. Bianchi and A. Serio, "Design and characterization of a fabric-based softness display," *IEEE Transactions on Haptics*, vol. 8, no. 2, pp. 152–163, April 2015.

[24] A. S. Moon, J. Garofalo, P. Koirala, M.-L. T. Vu, and L. Chuang, "Robotic surgery in gynecology," *Surgical Clinics of North America*, vol. 100, no. 2, pp. 445–460, apr 2020, robotic Surgery. [Online]. Available: http://www.sciencedirect.com/science/article/pii/S0039610919301653

[25] A. Giannini, M. Bianchi, D. Doria, S. Fani, M. Caretto, A. Bicchi, and T. Simoncini, "Wearable haptic interfaces for applications in gynecologic robotic surgery: a proof of concept in robotic myomectomy," *Journal of Robotic Surgery*, vol. 13, no. 4, pp. 585–588, may 2019.

[26] S. Fani, S. Ciotti, E. Battaglia, A. Moscatelli, and M. Bianchi, "W-FYD: A wearable fabric-based display for haptic multi-cue delivery and tactile augmented reality," *IEEE Transactions on Haptics*, vol. 11, no. 2, pp. 304–316, apr 2018.

[27] J. Konstantinova, K. Althoefer, P. Dasgupta, T. Nanayakkar *et al.*, "Salient features of soft tissue examination velocity during manual palpation," 2013.

[28] S. J. Lederman and R. L. Klatzky, "Relative availability of surface and object properties during early haptic processing." *Journal of Experimental Psychology: Human Perception and Performance*, vol. 23, no. 6, pp. 1680–1707, 1997.

[29] B. Hannaford and A. M. Okamura, "Haptics," in *Springer Handbook of Robotics*. Springer International Publishing, 2016, pp. 1063–1084.

[30] M. Bianchi, E. Battaglia, M. Poggiani, S. Ciotti, and A. Bicchi, "A wearable fabric-based display for haptic multi-cue delivery," in *2016 IEEE Haptics Symposium (HAPTICS)*. IEEE, April 2016, pp. 277–283.

[31] B. J. Davis, K. E. Haneke, K. Miner, A. Kowalik, J. C. Barrett, S. Peddada, and D. D. Baird, "The fibroid growth study: Determinants of therapeutic intervention," *Journal of Women's Health*, vol. 18, no. 5, pp. 725–732, may 2009.

[32] J. C. Gwilliam, Z. Pezzementi, E. Jantho, A. M. Okamura, and S. Hsiao, "Human vs. robotic tactile sensing: Detecting lumps in soft tissue," in *2010 IEEE Haptics Symposium*. IEEE, mar 2010, pp. 21–28.

[33] S. Condino, R. M. Viglialoro, S. Fani, M. Bianchi, L. Morelli, M. Ferrari, A. Bicchi, and V. Ferrari, "Tactile augmented reality for arteries palpation in open surgery training," in *Lecture Notes in Computer Science*. Springer International Publishing, 2016, pp. 186–197.

[34] C. Pacchierotti, A. Tirmizi, and D. Prattichizzo, "Improving transparency in teleoperation by means of cutaneous tactile force feedback," *ACM Transactions on Applied Perception*, vol. 11, no. 1, pp. 1–16, apr 2014.

[35] B. S. Peters, P. R. Armijo, C. Krause, S. A. Choudhury, and D. Oleynikov, "Review of emerging surgical robotic technology," *Surgical Endoscopy*, vol. 32, no. 4, pp. 1636–1655, feb 2018.

[36] A. Simorov, R. S. Otte, C. M. Kopietz, and D. Oleynikov, "Review of surgical robotics user interface: what is the best way to control robotic surgery?" *Surgical Endoscopy*, vol. 26, no. 8, pp. 2117–2125, feb 2012.

[37] E. Abdi, D. Kulic, and E. Croft, "Haptics in teleoperated medical interventions: Force measurement, haptic interfaces and their influence on user's performance," *IEEE Transactions on Biomedical Engineering*, vol. 67, no. 12, pp. 3438–3451, dec 2020.

[38] E. Afshari, M. Rostami, and F. Farahmand, "Review on different experimental techniques developed for recording force-deformation behaviour of soft tissues; with a view to surgery simulation applications," *Journal of Medical Engineering & Technology*, vol. 41, no. 4, pp. 257–274, jan 2017, pMID: 28140699. [Online]. Available: https://doi.org/10.1080/03091902.2016.1264492

[39] A. D. Russo, G. Fassini, S. Conti, M. Casella, A. D. Monaco, E. Russo, S. Riva, M. Moltrasio, F. Tundo, G. D. Martino, G. J. Gallinghouse, L. D. Biase, A. Natale, and C. Tondo, "Analysis of catheter contact force during atrial fibrillation ablation using the robotic navigation system: results from a randomized study," *Journal of Interventional Cardiac Electrophysiology*, vol. 46, no. 2, pp. 97–103, jan 2016.

[40] F. Ju, Y. Zhang, Y. Yun, H. Guo, X. Wei, C. Zhu, X. Zhang, D. Bai, and B. Chen, "A piezoelectric tactile sensor and human-inspired tactile exploration strategy for lump palpation in tele-operative robotic minimally invasive surgery," in *2019 IEEE International Conference on Robotics and Biomimetics (ROBIO)*. IEEE, dec 2019, pp. 223–228.

[41] A. S. Naidu, R. V. Patel, and M. D. Naish, "Low-cost disposable tactile sensors for palpation in minimally invasive surgery," *IEEE/ASME Transactions on Mechatronics*, vol. 22, no. 1, pp. 127–137, feb 2017.

[42] B. Li, Y. Shi, A. Fontecchio, and Y. Visell, "Mechanical imaging of soft tissues with a highly compliant tactile sensing array," *IEEE Transactions on Biomedical Engineering*, vol. 65, no. 3, pp. 687–697, mar 2018.

[43] M. Bianchi and A. Serio, "Design and characterization of a fabric-based softness display," *IEEE Transactions on Haptics*, vol. 8, no. 2, pp. 152–163, apr 2015.

[44] M. Bianchi, M. Poggiani, A. Serio, and A. Bicchi, "A novel tactile display for softness and texture rendering in tele-operation tasks," in *2015 IEEE World Haptics Conference (WHC)*. IEEE, jun 2015, pp. 49–56.

[45] J. Konstantinova, M. Li, G. Mehra, P. Dasgupta, K. Althoefer, and T. Nanayakkara, "Behavioral characteristics of manual palpation to localize hard nodules in soft tissues," *IEEE Transactions on Biomedical Engineering*, vol. 61, no. 6, pp. 1651–1659, jun 2014.

[46] J. B. Gafford, "Real-time parameter estimation of biological tissue using kalman filtering," pp. 1–11, 2018.